

Comparing Vibrotactile Stimulation to Combined Visual and Auditory Stimulation for 40 Hz Gamma Entrainment

Yeongdae Kim¹, Ayush Choudary¹, Hyeonseok Kim³,
Peter Teale², Brice McConnell²,
Mazen Al Borno^{1*}

¹Computer Science and Engineering, University of Colorado Denver | Anschutz Medical Campus, Colorado, USA.

²Department of Neurology, University of Colorado Denver | Anschutz Medical Campus, Colorado, USA.

³Division of Child and Adolescent Psychiatry, Cincinnati Children's Hospital Medical Center, OH, USA,

*Corresponding author. E-mail: mazen.alborno@ucdenver.edu

Contributing authors: yeongdae.kim@ucdenver.edu; ayush.choudhary@ucdenver.edu; hyeonseok.kim@cchmc.org; peter.teale@cuanschutz.edu; brice.mcconnell@cuanschutz.edu

Abstract

There is significant interest in combined visual and auditory stimulation to entrain 40 Hz gamma oscillations for the treatment of Alzheimer's disease and other neurological conditions such as stroke and insomnia. In this work, we compared another sensory modality—vibrotactile stimulation delivered with a glove—to visual and auditory stimulation in 15 healthy participants in terms of electroencephalogram (EEG) responses and subjective experience. We found that vibrotactile stimulation from the glove could evoke 40 Hz EEG responses in the central, frontal and, to a lesser extent, occipital cortices. Participants preferred the vibrotactile stimulation over the visual and auditory stimulation. Our study supports future investigations with vibrotactile stimulation for the treatment of neurological conditions.

Keywords: non-invasive stimulation, vibrotactile stimulation, Alzheimer's disease

Introduction

Alzheimer's disease (AD) is a neurodegenerative condition without an effective pharmacotherapeutic treatment that is estimated to affect 5.7 million people in the USA (Alzheimer's Association 2016) and 30-35 million people worldwide (Shin 2022). Brain oscillations are disrupted in AD and other neurological conditions such as Parkinson's disease and epilepsy. There is on-going research in developing non-invasive methods to restore physiological brain oscillations for these diseases (Soula et al., 2023). It has recently been found that non-invasive combined visual and auditory stimulation (VAS) at the gamma frequency of 40 Hz reduced pathologies associated with AD and improved cognitive function in mouse models of neurodegeneration (Adaikkan et al., 2019; Martorell et al., 2019). More specifically, stimulation at the 40 Hz gamma frequency, but not other frequencies, reduced the accumulation of Beta-amyloid plaques and phosphorylated tau protein that characterize AD (Manippa et al., 2022). Furthermore, six weeks of daily 1 hour of VAS reduced neuronal and synaptic loss, which are hallmarks of

neurodegenerative diseases. VAS had more beneficial effects than either visual or auditory stimulation alone, including decreasing amyloid in medial prefrontal cortex (Martorell et al., 2019). It is currently unclear whether visual stimulation with 40 Hz light flickering induces gamma entrainment in deep structures like the hippocampus, as conflicting results have been reported in the literature (Soula et al., 2023; Adaikkan et al., 2019). Another modality, namely somatosensory stimulation based on whole-body vibrotactile stimulation, also decreased brain pathology associated with AD in the primary somatosensory cortex and primary motor cortex (Suk et al., 2023). Other techniques such as vagal nerve stimulation can attenuate hippocampal amyloid load and improve cognition and memory in certain mouse models (Yu et al., 2023).

Based on these studies in mouse models, pilot studies in humans with AD are underway with VAS. Recent clinical studies show promising preliminary evidence that prolonged stimulation positively impacts neural activity and immune cells (Chan et al., 2022; He et al., 2021), as well as improves sleep quality and activities of daily living in patients with prodromal AD (Cimenser et al., 2021). The therapy consists of wearing neurostimulation glasses for an hour per day for months. In a randomized control trial, AD patients in the treatment group (n=46; receiving VAS from the glasses for a 6 month-period) showed reduced white matter and myelin loss compared to the sham group, as assessed with magnetic resonance imaging (Da et al., 2024). Participants wearing the neurostimulation glasses see flashes of light (i.e., light flickering) at 40 Hz, which causes them to have limited vision and prevents them from doing other activities during the therapy. In addition to the visual stimulation, participants receive an auditory tone at 40 Hz as well, which can also be difficult to tolerate and further restricts patient activity during therapy. In addition to AD, gamma oscillations induced by 40 Hz VAS can rescue functional synaptic plasticity after stroke in mice (Wang et al., 2023) and promote sleep in children with insomnia (Zhou et al., 2024). In this study, we investigated vibrotactile stimulation as a potential sensory modality for 40 Hz gamma entrainment. The mechanical vibratory input was applied on the back of the hand, which produces a sensation similar to a phone vibrating. We evaluated EEG responses from two minutes of VAS and vibrotactile stimulation on 15 healthy participants in terms of response locations and changes in brain connectivity. In addition, participants verbally answered a questionnaire to assess the tolerability of the different stimulation modalities.

Methods

Participants

15 healthy adult (4 females, age M = 28.6, SD = 6.7, Range 19–39) participants were recruited from the University of Colorado Denver community. With both verbal and written form explanation of the study requirements, all participants provided written informed consent, as approved by the Institutional Review Board at the University of Colorado Denver.

Experimental Setup

Each participant was first exposed to VAS, then to the vibrotactile stimulation. Each stimulation lasted for 2 minutes. We recorded EEG responses during the stimulation, and 2 minutes before (pre-stimulation) and after the stimulation (post-stimulation), resulting in a total of 6 minutes of recordings per sensory modality. We had a 5-minute rest period between the two stimulation modalities. Participants receiving the VAS were seated 2 feet away from the device. Participants were asked to keep their eyes open during VAS. For vibrotactile stimulation, participants wore gloves on their right hand and were asked to either keep their eyes open or closed for the whole experiment. Lastly, we conducted additional EEG recordings with VAS for 5 subjects on a different

day from the main experiment. In this session, we used an eight channel EEG headset (the OpenBCI Ultracortex 'Mark IV' EEG Headset) to increase the sampling rate from 125 Hz to 250 Hz and compute event-related potentials from VAS.

Stimulation devices

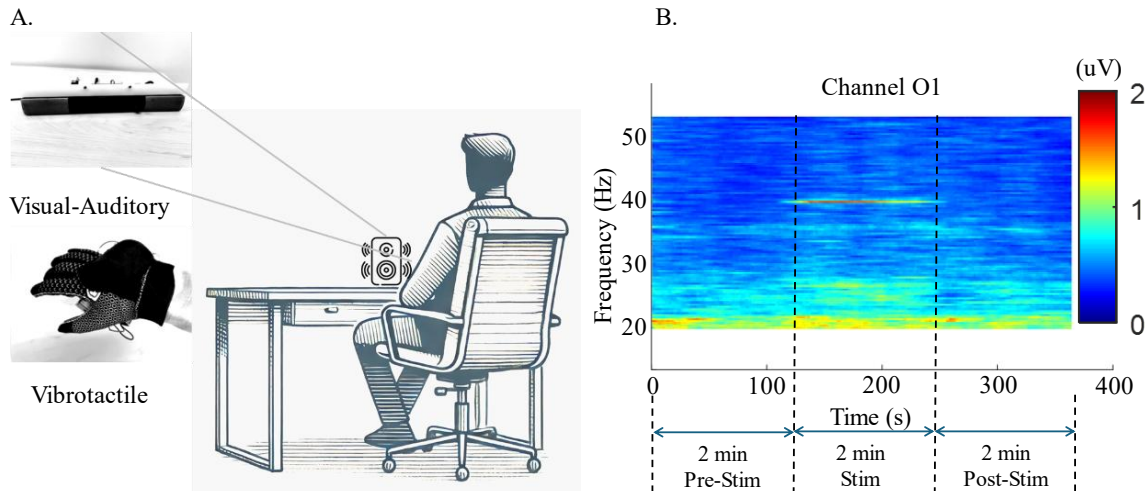


Figure 1. **A.** Illustration of the experimental session. Participants, sitting on a chair, receive VAS (visual-auditory stimulation) from a device on the desk. After a 5-minutes rest period, participants receive vibrotactile stimulation from a glove worn on their right hand. **B.** Time-frequency spectrogram of channel 'O1' from VAS. The stimulation is applied for two minutes, between 120-240 s. The stimulation causes a peak in power (uV) at the 40 Hz frequency.

Glove apparatus: The decision to design a glove for delivering vibrotactile stimulation stemmed from the rich concentration of sensory nerve endings and receptors in the human hand (Corniani et al., 2022). We used an Eccentric Rotating Mass (ERM) motor (Yootop 2300 RPM 12V DC motor) to achieve the desired 40 Hz frequency using a constant voltage (3.65 V). To maintain the constant voltage, we used a negative, adjustable linear voltage regulator (LM337T). We also used a dual differential comparator, a TO-220 heat sink, and multiple resistors. The comparator was incorporated to deactivate the circuit when input voltage fell below the minimum threshold required for optimal operation. The whole circuit was soldered onto a PCB board. The glove has three components, that is, the PCB board, the ERM motor and a 9V Lithium-ion battery. The PCB board and the motor are both placed inside a 3-D printed case. The motor was sewed onto the glove to stimulate the backside of the hand. We chose to stimulate the backside of the hand because it causes less interference with activities of daily living than the palm. Furthermore, our pilot testing indicated it was at least as effective for gamma entrainment as the palm. When constructing the glove apparatus, a stable frequency of 40 Hz was confirmed in two subjects in pilot testing. However, during the actual experiments, we observed a frequency variation of approximately 5%, ranging from 38 to 42 Hz. This deviation was caused by vibrations in the subject's hand and the motor itself attached to the glove. In future work, we will use an accelerometer to monitor the frequency in real time and adjust the voltage accordingly, rather than relying on a fixed voltage.

VAS apparatus: For VAS, a sound bar 'AS500' from Dell with a top mounted light source was used. The light source consisted of 36 Rextin LED of 5050 LEDs (5.0 x 5.0 mm, with three diodes per package), arranged in a rectangular bar with dimensions of 50 cm in length and 1.2 cm in width.

The audio input signal was split between the sound bar and a circuit to synchronously drive the LEDs. The input to the LED driver was high-pass filtered at 340 Hz and applied to an inverting op-amp with a gain of 20, which was sufficient to overload the amplifier, thus providing a negative output pulse to trigger a 555 timer. The timer was set to produce a 12.5 ms (50% duty cycle) positive pulse which was applied to a transistor switch in series with the LED power source. The audio stimulus was a 10 kHz tone burst of 1ms duration repeating at 40 Hz (Martorell et al., 2019). This was produced using an audio format file delivered by computer. The auditory stimuli were presented at 58 dB.

EEG setup

EEG signals were recorded using 16 dry electrodes from the OpenBCI Ultracortex 'Mark IV' EEG Headset, structured in a 10-20 configuration (see Fig. 2A). We used two references that were placed on the earlobes. The measured impedances ranged between 15 k Ω and 80 k Ω for all channels, which are below acceptable thresholds (Nuwer et al., 1998; Shad et al., 2020). The data sampling rate was 125 Hz. For one subject, whose head size did not fit the dry electrode headset, gel-type neuroelectric sensors were used instead.

EEG signal preprocessing

The EEG signals were imported into MATLAB 2022a (The MathWorks, Inc.) using EEGLAB v2024.0 (Delorme & Makeig, 2004). Sensor locations were assigned based on EEGLAB's default boundary element model from Dipfit v5.4 (Collins et al., 1994; Evans et al., 1993), and these standardized locations were later utilized for signal source analysis. EEG signals were filtered using a 60 Hz line noise filter (Bigdely-Shamlo et al., 2015) and finite impulse response (FIR) band-pass filter between 1-60 Hz. Re-referencing was performed to the average reference, with a zero-padded channel included to ensure the data retained full rank (Kim et al., 2023). Using the re-referenced EEG data, we computed 1-second quantized spectrograms and excluded data that showed atypical uniform increase across all frequencies, which can be caused by sensor dislocation, muscle activity or eye blinking (Cohen, 2014).

Following noise removal, independent component analysis (ICA) was deployed using AMICA (Palmer et al., 2012), which is an adaptive mixture ICA function to decompose the EEG data into mutually independent components (ICs) with corresponding topographic projections on the scalp sensors. The signal source dipole locations of ICs were then computed using Dipfit, which localized each IC within the Montreal neurological institute template (Tzourio-Mazoyer et al., 2002). Each of the dipole locations, initially represented as a single 2x2x2 mm voxel, was transferred into a dipole density sphere through 3-dimensional Gaussian smoothing with a 20-mm full width at half maximum. This transformation was applied to mitigate inter-subject variability in dipole locations, allowing for the identification of activation patterns across specific anatomical regions. The resulting dipole density was mapped onto anatomical regions using an automated anatomical labeling system, enabling consistent localization across subjects and group-level analysis (Loo et al., 2019).

EEG signal analysis

We analyzed the relative intensity changes between the stimulation and pre-stimulation periods to examine whether brainwave entrainment occurred and in which locations it activated the most. A paired t-test was performed on the relative intensity at the 40 Hz frequency between the stimulation and pre-stimulation periods. We also investigated the EEG connectivity shift from the stimulation. To compute the average effective connectivity across ICs for each group, the renormalized partial directed coherence (RPDC) was calculated using time-frequency

decomposition. This analysis was conducted at a sampling rate of 125 Hz, and 45 frequency bins logarithmically spaced between 2 and 50 Hz with single-window analysis for pre-, post-, and during stimulation periods. This process produced a connectivity matrix of varying number of IC \times IC for each subject per three periods. Lastly, weak family-wise error rate (FWER) control was applied to analyze the statistical significance of changes in time–frequency decomposed RPDC across the pre-, during and post-stimulation periods.

Results

We compared the effects of the different stimulation modalities on the neural circuit based on the entrainment location on the scalp at the 40 Hz stimulation frequency. In Fig. 2, we illustrate the relative intensity of stimulation onset brain entrainment at the 40 Hz frequency compared to the pre-stimulation period, averaged over all subjects, for VAS and vibrotactile stimulation. As shown in Fig. 2B–E, the primary response of the VAS was the occipital area with a 5.3 ± 3.0 dB intensity increase at the O2 sensor. In Fig. 2C, we show the 40 Hz response in O2 during the pre-

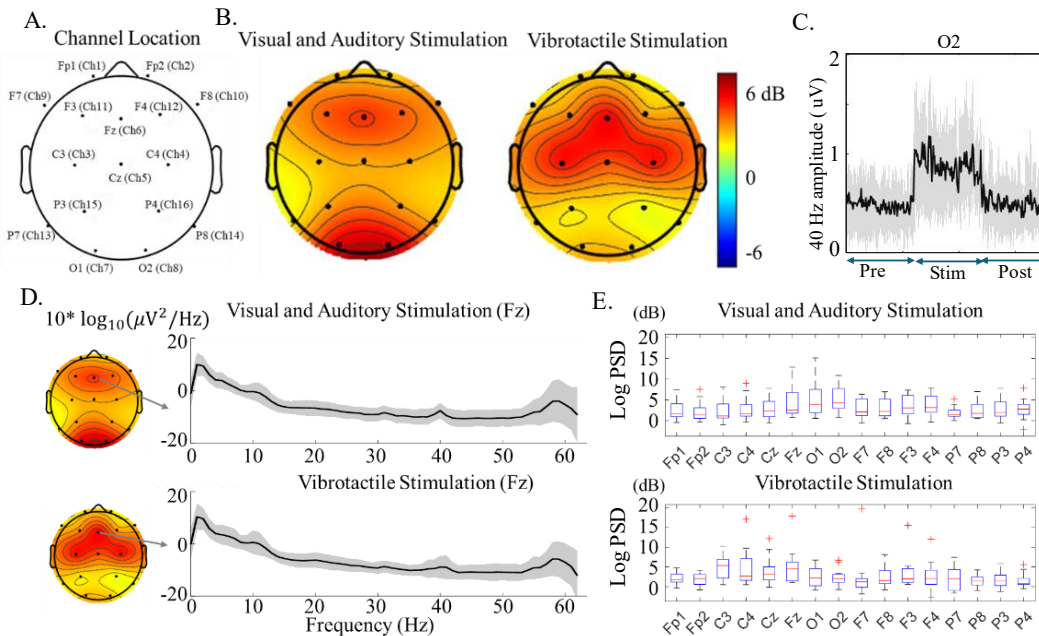


Figure 2. **A.** Sensor locations on the scalp in our EEG study with 16 channels. **B.** Respective brainwave entrainment for each stimulation modality. The size of the entrainment is represented by the relative increase in intensity compared to the pre-stimulation period, displayed on a dB scale. The colors represent the relative intensity of stimulation onset brain entrainment from the 40 Hz stimulation frequency compared to the pre-stimulation period. **C.** Time series of the 40 Hz response during the experiment for sensor O2 from VAS. The black solid line represents the average across all participants, and the gray shading indicates on standard deviation from the mean. **D.** Log Power Spectral Density of the pre-dominantly entrained channel Fz from the two stimulation modalities. **E.** Boxplots of channel-specific brainwave entrainment (dB) for VAS (top) and vibrotactile stimulation (bottom).

stimulation, stimulation and post-stimulation periods. The other main response occurred in the frontal cortices adjacent to channel Fz with a 4.2 ± 3.4 dB intensity increase. Vibrotactile stimulation showed the highest entrainment on the frontal-central region with an average 4.8 ± 4.3 dB intensity on sensor Fz. The second most entrained sensor is C3 in the left hemisphere, as

participants wore gloves on their right hand. Nearly half of the participants ($n=7$) demonstrated strong entrainment in the occipital and adjacent parietal regions in response to vibrotactile stimulation (with more than 3 dB intensity increase).

We excluded the possibility that this entrainment was due to the mechanical vibration of the motor, as we verified that the accelerometer (placed near the occipital regions) did not exhibit a peak at

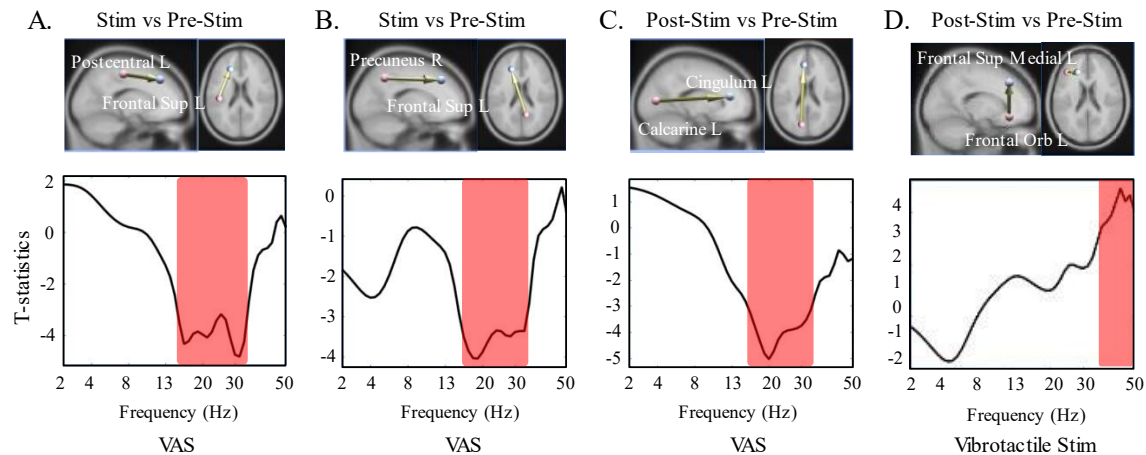


Figure 3. A. Connectivity shift measures with VAS (comparing the stimulation and pre-stimulation periods) in the 13-30 Hz frequency band between the left postcentral gyrus and left superior frontal cortex, depicted in a connectome connectivity map. The red-highlighted regions of the frequencies indicate t-statistics with an absolute value greater than 3 ($|t(14)| > 3$, $p < .01$). **B.** Same as A except the regions are the right precuneus and the left superior frontal cortex. **C.** Same as A except the comparisons are between the post-stimulation and pre-stimulation periods, and the regions are the left calcarine and left cingulum. **D.** Same as C except that it is for vibrotactile stimulation, and the regions are the left superior medial frontal gyrus and the left orbital frontal region.

the 40 Hz frequency. In Fig. 2D, we show the power spectral density mean and standard deviation on a predominantly entrained channel (Fz). The response amplitude to the vibrotactile stimulation was larger than that of the VAS. However, variations in the motor frequency (between 38-42 Hz due to the glove apparatus) resulted in a more widespread response near the 40 Hz target. No 40-Hz entrainment was observed in the post-stimulation condition for VAS and vibrotactile stimulation. Using weak FWER control, we identified statistically significant connectivity shifts from VAS and vibrotactile stimulation. Statistical analyses were performed across three periods (pre-, during and post-stimulation) for the two stimulation modalities. Significant differences were observed between the stimulation and pre-stimulation periods, and between the post- and pre-stimulation periods. During stimulation, connectivity from the parietal regions (specifically the postcentral gyrus and the precuneus) to the frontal regions decreased in the beta band (13-30 Hz) compared to the pre-stimulation period (Fig. 3A-B). A similar pattern of decreased connectivity was observed after stimulation, though in a different anatomical location, specifically from the left calcarine to left cingulum (Fig. 3C). This preserved frequency-specific modulation across different anatomical pathways suggests a broader beta-band reorganization of anterior-posterior connectivity patterns following stimulation. Following vibrotactile stimulation, we observed a significant increase in connectivity between the left superior medial frontal gyrus and the left orbital frontal region compared to the pre-stimulation period (see Fig. 3D). This change in connectivity was observed in the gamma band, which corresponds to the stimulation frequency (around 40 Hz).

We conducted verbal interviews with participants after undergoing the experiment. Their assessments of each stimulation modality are summarized in Table 1. Participants were asked to evaluate how long they can receive the stimulation on a daily basis for months and rate their tolerance on a scale from 0 to 10, where 0 indicated extreme difficulty in tolerating the stimulation and 10 indicated no difficulty. The tolerance scores for VAS and vibrotactile stimulation were 6.2 ± 2.0 and 8.8 ± 1.3 respectively, showing higher tolerance for the vibrotactile stimulation ($p < .01$). All participants indicated higher daily duration tolerance for vibrotactile stimulation ($67.7 \text{ min} \pm 75.8$) compared to VAS ($11.5 \text{ min} \pm 15.4$; $p < .01$). Participants reported experiencing eyesight blurring from the visual stimulation, finding the auditory stimulation to be the most irritating sensory modality, and feeling bored during VAS. The consensus was that vibrotactile stimulation is the more tolerable stimulation modality, causing the least discomfort.

Table 1. Participants verbal responses to the stimulation modality.

Stimulation Type	Visual and Auditory	Vibrotactile	<i>P</i> -value
Tolerance (0: intolerable / 10: tolerable)	6.2 ± 2.4	8.8 ± 1.3	$<.01$
Daily Duration Tolerance (minutes)	11.5 ± 15.4	67.7 ± 75.8	$<.01$
Preferred Modality (15 subjects)	1/15	14/15	

In Fig. 4, we computed the event-related potentials for one subject during 2 minutes of VAS (26 samples per 100 ms epoch). We observe that among the seven EEG channels fluctuating at 40 Hz, two channels from the occipital region showed more than double the amplitude and were antiphase with the other channels. We found that 2 out of 5 participants had this approximate π phase difference between the occipital and other entrained cortices. We could not reliably estimate the phase difference in the remaining subjects because the sampling rate was still too low.

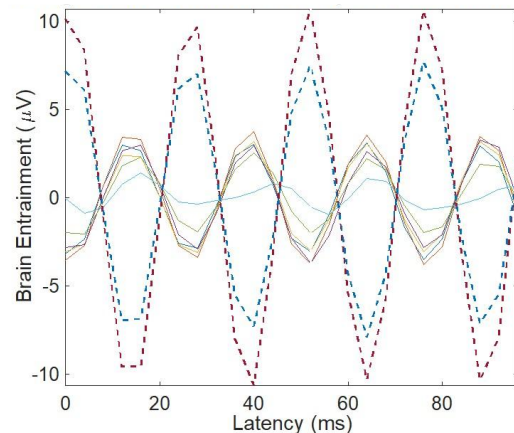


Figure 4. Event-related potentials for one subject during VAS. Solid lines represent the prefrontal, frontal and central cortex and dotted lines represent the occipital cortex.

Discussion

Non-invasive 40 Hz stimulation has recently received considerable attention because of promising experiments conducted on mouse models of neurodegeneration (Adaikkan et al., 2019; Martorell et al., 2019) and stroke (Wang et al., 2023). Several studies are now underway in AD patients to assess the feasibility and safety of VAS and to assess the effects of the stimulation when applied over long durations on the neural circuitry (Chan et al., 2022; He et al., 2021; Cimenser et al., 2021). In this study, we examined EEG responses from healthy participants to VAS and vibrotactile stimulation and gathered participants' feedback on their preferred stimulation modality.

Our experiments confirmed 40 Hz brainwave entrainment with VAS and vibrotactile stimulation. Teplan et al., 2011 demonstrated "short-lived" brainwave entrainment in the occipital and frontal cortex regions across multiple frequencies (2, 4, 9 and 17 Hz). We observed similar entrainment in these regions with 40 Hz VAS. In addition to the O1-O2 channels, VAS induced F3, Fz and

F4—regions associated with the dorsolateral and medial frontal cortices—indicating the involvement of attention and sensory processing in response to the combined stimuli. In contrast, vibrotactile stimulation primarily induced C3, Cz, and C4 in the sensorimotor cortex, associated with processing tactile and proprioceptive information. A prior study found that vibrotactile stimulation decreased brain pathology in these regions in mouse models of neurodegeneration (Suk et al., 2023). Vibrotactile stimulation had smaller responses in the frontal cortices than VAS, perhaps due to the reduced attentional involvement demands of the stimulation. Furthermore, vibrotactile stimulation exhibited strong occipital responses in seven out of fifteen participants, consistent with prior work showing the activation of occipital cortex during tactile processing (Marabet et al., 2007; Zangaladze et al., 1999). Similarly, VAS also entrained the somatosensory cortices (see Fig. 2A), which may encode visual information in working memory (Christophel & Haynes 2014).

During VAS, we found that pathway-relevant connectivity from the occipital area to the frontal area decreased (Murray et al., 2011; see Fig. 3A-C). Given that no other significant shifts in connectivity were observed, this suggests that the 40 Hz VAS may have induced beta signals originating directly from the frontal area, reducing connectivity with other regions. Alternatively, it could be that the mere repetitive 40 Hz stimulus, lacking significant cognitive meaning, led to a suppression of beta band connectivity. Furthermore, this changed connectivity persisted after the stimulation (i.e., the occipital-frontal beta band connectivity reductions observed during stimulation remained present post-stimulation). In contrast, vibrotactile stimulus increased interconnectivity within the frontal region in the gamma band (the stimulus frequency) at the post-stimulation period. No change in circuit connectivity was found post-stimulation with VAS in the gamma band.

Prior work has shown that VAS is more effective than visual or auditory stimulation alone in reducing AD pathologies (Martorell et al., 2019). The brain adjusts for the differences in transmission and sensory processing times when integrating different sensory modalities (Fujisaki et al., 2004). Teplan et al., 2009 investigated VAS and observed a stabilized angular difference after a certain period of sustained stimulation. We also found a phase difference between the auditory and visual stimulation entrainment (see Fig. 4). Future studies should investigate the optimal lags (if any) between sensory modalities to avoid negative interference at 40 Hz and improve treatment outcomes, which will be especially as technologies with more sensory modalities are developed.

In terms of the participants' feedback to stimulation, all but one participant preferred the vibrotactile stimulation modality. The participant who preferred VAS also noted that the vibrotactile stimulation would likely be easier to tolerate if applied on a daily basis. Since the stimulation would likely require daily sessions over months or even years, treatments can be a burden on some individuals. Therefore, vibrotactile stimulation may serve as a complementary (e.g., by replacing some VAS duration with vibrotactile stimulation) or an alternative sensory modality to VAS, offering greater comfort and mobility, and reducing limitations on social interactions and engagement with the external environment. Moreover, for individuals with reflex epilepsies, such as photosensitive occipital lobe epilepsy, non-visual stimuli options may minimize risk. The incorporation of other stimulation modalities could help address the diverse needs of patients and enhance treatment outcomes. Extending treatment duration and improving compliance through such options may also be critical for promoting neural plasticity and supporting recovery.

REFERENCES

Adaikkan, C., Middleton, S. J., Marco, A., Pao, P.-C., Mathys, H., Kim, D. N.-W., Gao, F., Young, J. Z., Suk, H.-J., Boyden, E. S., McHugh, T. J., & Tsai, L.-H. (2019). Gamma Entrainment Binds Higher-Order Brain Regions and Offers Neuroprotection. *Neuron*, 102(5), 929-943.e8. <https://doi.org/10.1016/j.neuron.2019.04.011>

Alzheimer's Association. (2018). 2018 Alzheimer's disease facts and figures. *Alzheimer's & Dementia*, 14(3), 367-429. <https://doi.org/10.1016/j.jalz.2018.02.001>

Bier, N., Van Der Linden, M., Gagnon, L., Desrosiers, J., Adam, S., Louveaux, S., & Saint-Mleux, J. (2008). Face-name association learning in early Alzheimer's disease: A comparison of learning methods and their underlying mechanisms. *Neuropsychological Rehabilitation*, 18(3), 343-371. <https://doi.org/10.1080/09602010701694723>

Bigdely-Shamlo, N., Mullen, T., Kothe, C., Su, K.-M., & Robbins, K. A. (2015). The PREP pipeline: Standardized preprocessing for large-scale EEG analysis. *Frontiers in Neuroinformatics*, 9. <https://doi.org/10.3389/fninf.2015.00016>

Chan, D., Suk, H.-J., Jackson, B. L., Milman, N. P., Stark, D., Klerman, E. B., Kitchener, E., Fernandez Avalos, V. S., De Weck, G., Banerjee, A., Beach, S. D., Blanchard, J., Stearns, C., Boes, A. D., Uitermarkt, B., Gander, P., Howard, M., Sternberg, E. J., Nieto-Castanon, A., ... Tsai, L.-H. (2022). Gamma frequency sensory stimulation in mild probable Alzheimer's dementia patients: Results of feasibility and pilot studies. *PLOS ONE*, 17(12), e0278412. <https://doi.org/10.1371/journal.pone.0278412>

Christophel, Thomas B., and John-Dylan Haynes. "Decoding complex flow-field patterns in visual working memory." *Neuroimage* 91 (2014): 43-51.

Cimenser, A., Hempel, E., Travers, T., Strozewski, N., Martin, K., Malchano, Z., & Hajós, M. (2021). Sensory-Evoked 40-Hz Gamma Oscillation Improves Sleep and Daily Living Activities in Alzheimer's Disease Patients. *Frontiers in Systems Neuroscience*, 15, 746859. <https://doi.org/10.3389/fnsys.2021.746859>

Cohen, M. X. (Ed.). (2014). *Analyzing neural time series data: Theory and practice*. The MIT Press.

Corniani, G., & Saal, H. P. (2020). Tactile innervation densities across the whole body. *Journal of Neurophysiology*, 124(4), 1229-1240.

Da, Xiao, et al. "Noninvasive gamma sensory stimulation may reduce white matter and myelin loss in Alzheimer's disease." *Journal of Alzheimer's Disease* 97.1 (2024): 359-372.

Fekedulegn, D., Andrew, M. E., Shi, M., Violanti, J. M., Knox, S., & Innes, K. E. (2020). Actigraphy-Based Assessment of Sleep Parameters. *Annals of Work Exposures and Health*, 64(4), 350-367. <https://doi.org/10.1093/annweh/wxaa007>

Fujisaki, Waka, et al. "Recalibration of audiovisual simultaneity." *Nature neuroscience* 7.7 (2004): 773-778.

Galasko, D., Bennett, D., Sano, M., Ernesto, C., Thomas, R., Grundman, M., & Ferris, S. (1997). An inventory to assess activities of daily living for clinical trials in Alzheimer's disease. The Alzheimer's Disease Cooperative Study. *Alzheimer Disease and Associated Disorders*, 11 Suppl 2, S33-39.

Habibzadeh Tonekabony Shad, E., Molinas, M., & Ytterdal, T. (2020). Impedance and Noise of Passive and Active Dry EEG Electrodes: A Review. *IEEE Sensors Journal*, 20(24), 14565-14577. <https://doi.org/10.1109/JSEN.2020.3012394>

He, Q., Colon-Motas, K. M., Pybus, A. F., Piendel, L., Seppa, J. K., Walker, M. L., Manzanares, C. M., Qiu, D., Miocinovic, S., Wood, L. B., Levey, A. I., Lah, J. J., & Singer, A. C. (2021). A feasibility trial of gamma sensory flicker for patients with prodromal Alzheimer's disease. *Alzheimer's & Dementia: Translational Research & Clinical Interventions*, 7(1), e12178. <https://doi.org/10.1002/trc2.12178>

Kim, H., Luo, J., Chu, S., Cannard, C., Hoffmann, S., & Miyakoshi, M. (2023). ICA's bug: How ghost ICs emerge from effective rank deficiency caused by EEG electrode interpolation and incorrect re-referencing. *Frontiers in Signal Processing*, 3, 1064138. <https://doi.org/10.3389/frsip.2023.1064138>

Koshiyama, D., Miyakoshi, M., Joshi, Y. B., Molina, J. L., TanakaKoshiyama, K., Sprock, J., Braff, D. L., Swerdlow, N. R., & Light, G. A. (2020). Abnormal effective connectivity underlying auditory mismatch negativity impairments in schizophrenia. *Biological Psychiatry: Cognitive Neuroscience and Neuroimaging*, 5, 1028–1039.

Loo, S. K., Miyakoshi, M., Tung, K., Lloyd, E., Salgari, G., Dillon, A., Chang, S., Piacentini, J., & Makeig, S. (2019). Neural activation and connectivity during cued eye blinks in Chronic Tic Disorders. *NeuroImage: Clinical*, 24, 101956. <https://doi.org/10.1016/j.nicl.2019.101956>

Mander, B. A., Marks, S. M., Vogel, J. W., Rao, V., Lu, B., Saletin, J. M., Ancoli-Israel, S., Jagust, W. J., & Walker, M. P. (2015). β -amyloid disrupts human NREM slow waves and related hippocampus-dependent memory consolidation. *Nature Neuroscience*, 18(7), 1051–1057. <https://doi.org/10.1038/nn.4035>

Manippa, Valerio, et al. "An update on the use of gamma (multi) sensory stimulation for Alzheimer's disease treatment." *Frontiers in Aging Neuroscience* 14 (2022): 1095081.

Martorell, A. J., Paulson, A. L., Suk, H.-J., Abdurrob, F., Drummond, G. T., Guan, W., Young, J. Z., Kim, D. N.-W., Kritskiy, O., Barker, S. J., Mangena, V., Prince, S. M., Brown, E. N., Chung, K., Boyden, E. S., Singer, A. C., & Tsai, L.-H. (2019). Multi-sensory Gamma Stimulation Ameliorates Alzheimer's-Associated Pathology and Improves Cognition. *Cell*, 177(2), 256-271.e22. <https://doi.org/10.1016/j.cell.2019.02.014>

McConnell, B. V., Kaplan, R. I., Teale, P. D., Kronberg, E., Broussard, J. L., Guzetti, J. R., Sillau, S. H., Dhanasekaran, A. R., Kluger, B. M., & Berman, B. D. (2019). Feasibility of home-based automated transcranial electrical stimulation during slow wave sleep. *Brain Stimulation*, 12(3), 813–815. <https://doi.org/10.1016/j.brs.2019.02.014>

McConnell, B. V., Kronberg, E., Teale, P. D., Sillau, S. H., Fishback, G. M., Kaplan, R. I., Fought, A. J., Dhanasekaran, A. R., Berman, B. D., Ramos, A. R., McClure, R. L., & Bettcher, B. M. (2021). The aging slow wave: A shifting amalgam of distinct slow wave and spindle coupling subtypes define slow wave sleep across the human lifespan. *Sleep*, 44(10), zsab125. <https://doi.org/10.1093/sleep/zsab125>

Murray, M. M., & Wallace, M. T. (Eds.). (2012). *The neural bases of multisensory processes*. CRC Press.

Nuwer, M. R., Comi, G., Emerson, R., Fuglsang-Frederiksen, A., Guérit, J.-M., Hinrichs, H., Ikeda, A., Jose C. Lucas, F., & Rappelsburger, P. (1998). IFCN standards for digital recording of clinical EEG. *Electroencephalography and Clinical Neurophysiology*, 106(3), 259–261. [https://doi.org/10.1016/S0013-4694\(97\)00106-5](https://doi.org/10.1016/S0013-4694(97)00106-5)

Palmer, J. A., Kreutz-Delgado, K., & Makeig, S. (2012). AMICA: An adaptive mixture of independent component analyzers with shared components. Swartz Center for Computational Neuroscience, University of California San Diego, Tech. Rep. 1-15.

Shad, Erwin Habibzadeh Tonekabony, Marta Molinas, and Trond Ytterdal. "Impedance and noise of passive and active dry EEG electrodes: a review." *IEEE Sensors Journal* 20, no. 24 (2020): 14565-14577.

Shin, Joon-Ho. "Dementia epidemiology fact sheet 2022." *Annals of Rehabilitation Medicine* 46.2 (2022): 53-59.

Suk, H. J., Buie, N., Xu, G., Banerjee, A., Boyden, E. S., & Tsai, L. H. (2023). Vibrotactile stimulation at gamma frequency mitigates pathology related to neurodegeneration and improves motor function. *Frontiers in Aging Neuroscience*, 15, 1129510.

Soula, M., Maslarova, A., Harvey, R. E., Valero, M., Brandner, S., Hamer, H., Fernández-Ruiz, A., & Buzsáki, G. (2023). Interictal epileptiform discharges affect memory in an Alzheimer's disease mouse model. *Proceedings of the National Academy of Sciences*, 120(34), e2302676120. <https://doi.org/10.1073/pnas.2302676120>

Teplan, M., Palus, M., & Vejmelka, M. (2010). EEG phase synchronization and information flow during audio-visual stimulation. 2010 3rd International Symposium on Applied Sciences in Biomedical and Communication Technologies (ISABEL 2010), 1–4. <https://doi.org/10.1109/ISABEL.2010.5702888>

Teplan, M., Krakovská, A., & Štolc, S. (2011). Direct effects of audio-visual stimulation on EEG. *Computer Methods and Programs in Biomedicine*, 102(1), 17–24. <https://doi.org/10.1016/j.cmpb.2010.11.013>

Tzourio-Mazoyer, N., Landeau, B., Papathanassiou, D., Crivello, F., Etard, O., Delcroix, N., Mazoyer, B., & Joliot, M. (2002). Automated anatomical labeling of activations in SPM using a macroscopic anatomical parcellation of the MNI MRI single-subject brain. *NeuroImage*, 15, 273–289. <https://doi.org/10.1006/nimg.2001.0978>

Wang, C., Lin, C., Zhao, Y., Samantzis, M., Sedlak, P., Sah, P., & Balbi, M. (2023). 40-Hz optogenetic stimulation rescues functional synaptic plasticity after stroke. *Cell reports*, 42(12).

Williams, A. M., Angeloni, C. F., & Geffen, M. N. (2023). Sound Improves Neuronal Encoding of Visual Stimuli in Mouse Primary Visual Cortex. *The Journal of Neuroscience*, 43(16), 2885–2906. <https://doi.org/10.1523/JNEUROSCI.2444-21.2023>

Yu, Yutian, et al. "Transauricular vagal nerve stimulation at 40 Hz inhibits hippocampal P2X7R/NLRP3/caspase-1 signaling and improves spatial learning and memory in 6-month-old APP/PS1 mice." *Neuromodulation: Technology at the Neural Interface* 26.3 (2023): 589-600.

Zhou, X., He, Y., Xu, T., Wu, Z., Guo, W., Xu, X., ... & Chen, J. F. (2024). 40 Hz light flickering promotes sleep through cortical adenosine signaling. *Cell Research*, 34(3), 214-231.

Supplementary information. All the de-identified data from our study and code are available at <https://doi.org/10.5281/zenodo.15008933>

Acknowledgements. We are grateful for the Coleman Institute for Cognitive Disabilities and ARIAD CU Denver for funding this work.

Declarations

Appendix